

pubs.acs.org/acsapm Article

# Local Viscosity of Interfacial Layers in Polymer Nanocomposites Measured by Magnetic Heating

Di Wu, Donovan G. Weiblen, Rahmi Ozisik, and Pinar Akcora\*



Cite This: https://dx.doi.org/10.1021/acsapm.0c00889



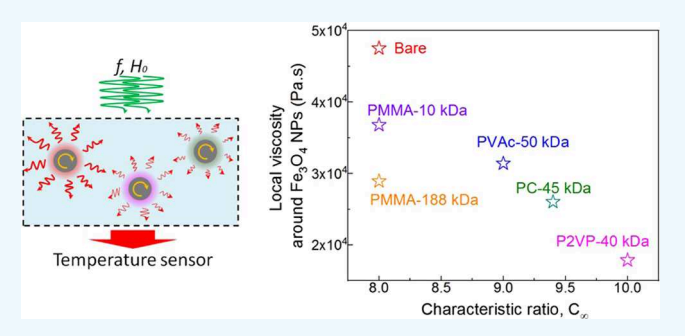
**ACCESS** 

III Metrics & More

Article Recommendations

SI Supporting Information

ABSTRACT: The strength of interfacial attractions between polymer chains and nanoparticles is known to control the mobility of chains and viscoelastic properties in polymer nanocomposites. We chose the interfacial layers around magnetic nanoparticles to consist of two different miscible polymers and measured the energy absorption rates as particles dissipate energy while they rotate under a high-frequency alternating magnetic field. Local viscosities were calculated from the measured rotational relaxation times using the classical absorption model. The changes in local viscosities were attributed to the rigidity of adsorbed polymers and chemical heterogeneities of their interfacial layers. The highest viscosity was



measured with the flexible, shorter adsorbed poly(methyl methacrylate) chains. The weak interphases between poly(methyl acrylate) and highly rigid polymers such as poly(2-vinyl pyridine), and poly(bisphenol A carbonate) allowed particles to rotate easily in a diffusive mode, yielding the lowest viscosity that matched to the viscosity prediction of an unentangled matrix polymer. Chemical and dynamic heterogeneity of interfacial layers around nanoparticles highly depend on the rigidity of chains. Measuring the local viscosity of interfacial polymer layers is essential for interfacial layer-controlled mechanisms of stress transfer, reinforcement, and thermal conductivity in polymer nanocomposites.

KEYWORDS: polymer nanocomposite, magnetic heating, viscosity, interfacial layer, chemical heterogeneity

## INTRODUCTION

Polymer-coated and functionalized nanoparticles have been widely used to achieve good dispersion in polymer nanocomposites. Dynamics and glass transition temperature of bound interfacial layers on nanoparticles have been investigated to understand the effect of interfacial relaxations of chains, as these interfacial layers govern mechanical properties and reinforcement in nanocomposites. 1-3 Interfacial polymer attractions and entanglements can be modified by adsorbed and matrix polymer chemistries and chain lengths.4-Subsequently, dynamics of chemically different polymers on nanoparticles becomes critical and can be used for enhancing the mechanical adaptivity of polymer nanocomposites upon temperature changes or under shear. The dynamic asymmetry in miscible blends such as poly(ethylene oxide) (PEO), and poly(methyl methacrylate) (PMMA) has been extensively studied to optimize their mechanical and ion-conducting properties; 8-13 however, this dynamic asymmetry effect has not been studied around nanoparticles or within confined regions. Polymer blends with different glass transition temperatures (Tgs) offer an unusual viscoelastic response when high  $T_{\rm g}$  polymer is adsorbed on nanoparticles.

In our previous studies, we showed that PMMA-adsorbed SiO<sub>2</sub> nanoparticles, which were dispersed in PEO, exhibited stiffening behavior as temperature swept across the T<sub>2</sub> of

PMMA. 14,15 The observed elastic hysteresis with increasing temperature confirmed that adsorbed chains on nanoparticles were stable after several heating-cooling cycles and the thermal-softening was reversible. We attribute this response to the unusual fast dynamics of disentangled PEO chains, as they are confined within the glassy adsorbed PMMA chains at low temperatures. To understand the effect of  $T_{_{g}}$  differences  $(\Delta T_{s})$  between adsorbed and matrix polymers on the observed stiffening behavior, we have prepared poly(methyl acrylate) (PMA) nanocomposites using poly(vinyl acetate) (PVAc) adsorbed nanoparticles.<sup>7</sup> PMA–PVAc is a miscible blend system with a small  $\Delta T_{_g}$  of 25 °C. The system with a small  $\Delta T_{_g}$ does not contain differences in chain dynamics and reptation times; thus, we did not expect to measure thermal stiffening in PMA-PVAc. Interestingly, however, reinforcement was enhanced with the use of short (40 kDa) PMA matrix chains as compared to long PMA chains (140 kDa). Temperature

Received: August 15, 2020 Accepted: October 20, 2020



sweep experiments on the same samples also showed that composites with the short PMA matrix chains stiffened more than those containing long PMA chains. The reinforcement of this composite was attributed to good mixing and polar interactions between the short matrix and adsorbed chains within the interphase volume. These factors reveal the role of interfacial chain packing within the interphases on the viscoelastic response and the effective bridging formed by the adsorbed chains. Further measurements with X-ray photon correlation spectroscopy confirmed that particles slowed down in the network forming a composite, which was found to be consistent with the rheological observations. Other works also supported these results and showed that the mass density of interfacial layers and interfacial reinforcement increased with decreasing matrix molecular weight and the rigidity of both matrix and adsorbed chains. 16-18

The viscoelastic properties of interfacial layers in polymer nanocomposites can be measured by atomic force microscopy (AFM). <sup>17,19,20</sup> Techniques of fluctuation correlation spectroscopy<sup>21</sup> or elastic recoil detection<sup>22</sup> probe diffusion of nanoparticles within a polymer at the zero-shear viscosity limit at long times. It was shown that noninteracting particles with sizes smaller than the radius of gyration of the matrix polymer deviated from translational diffusion. <sup>21,23,24</sup> At short times, the particle displacement was not affected by entanglements. <sup>25</sup>

Here, we measured the interfacial local viscosity through magnetic heating of rotating particles. Rotational particle motion occurs without displacements, unlike translational motion. Therefore, the rotation of the probe particle is expected to be less affected by the polymer entanglement network. We investigate the role of polymer rigidity and chain length on the viscosity of composites to better understand the role of interfacial layers on the overall mechanical response of the polymer nanocomposites. Interestingly, the effect of weak and strong interphase layers in PMA nanocomposites on their interfacial viscosities is verified with the low and high viscosity values, respectively. The existence of chemically different miscible polymers in interfacial layers, as shown in this work, governs the local viscosity through chain rigidity, which controls the entanglement of interfacial chains. Chemical heterogeneity of polymers around nanoparticles suggests the dynamics of polymers at different time scales, which can be used to enhance the melt properties of polymer nanocomposites, and their mechanical stability for high-temperature applications.

### EXPERIMENTAL SECTION

Surface Modification of Fe $_3$ O $_4$  Nanoparticles. Fe $_3$ O $_4$  nanoparticles (NPs) with 15 nm diameter were purchased from Rosecreek Technologies Inc. Four hundred milligrams of NPs were mixed with 45 mL of deionized (DI) equimolar water/ethanol mixture in a 100 mL two-neck flask. The colloidal solution was stirred under continuous nitrogen flow for 1 h. Then, the solution was bath-sonicated for another 30 min. After that, 0.8 mL of (3-aminopropyl)-triethoxysilane (APTES), which was purchased from Sigma-Aldrich, was added to the NP solution and the reaction was let to proceed at 40 °C under nitrogen for 12 h. Amine-functionalized NPs (bare NPs) were collected after centrifuging and washing three times with acetone and DI water and tested in the Bruker Tensor 27 Fourier transform infrared (FTIR) spectrometer to confirm the silane modification of particles (Figure S1).

PMMA at two different molecular weights, 10 and 188 kDa, with a polydispersity index of 1.2 was synthesized via atom transfer radical

polymerization (ATRP) in our laboratory. PVAc (50 kDa) was dissolved in acetonitrile, and P2VP (40 kDa) and PC (45 kDa) were dissolved in dichlorobenzene. The concentration of the polymer was kept constant at 15 mg/mL for all polymers. Bare Fe<sub>3</sub>O<sub>4</sub> was added to the polymer solution at a particle concentration of 5 mg/mL. The solution was sonicated for 10 min and then stirred for 30 min. Polymer-adsorbed NPs were collected by centrifugation and washed several times with the corresponding solvent to remove all free residual polymers. The particles were dried again under vacuum at room temperature. The characteristic ratios ( $C_{\infty}$ ) and the amounts of adsorbed polymers (as mass percent and as number of chains per nanoparticle) are summarized in Table 1. Solubility of adsorbed and

Table 1. Characteristics of the Adsorbed Polymers on Nanoparticles

	molecular weight		mass fraction <sup>a</sup>	chain number density
polymer	(kDa)	$C_{\infty}$	(wt %)	(#chains/NP)
PMMA	10	8	2.78	16
PMMA	188	8	9.80	3
PVAc	50	9	4.01	4
PC	45	9.4	4.38	5
P2VP	40	10	5.29	7
PMA (matrix)	40	8		

<sup>&</sup>quot;Measured via thermal gravimetric analysis (TGA) experiments (see Figure S2).

matrix polymers is important parameter to achieve good particle dispersion and compatibility of the interphases. All polymer pairs used in this study are miscible, and their interaction parameters are provided in the Supporting Information.

**Preparation of Nanocomposites.** PMA was dissolved in acetonitrile to form a solution with 15 mg/mL concentration. Polymer-coated NPs were added to the PMA solution to achieve a nanoparticle concentration of 30% by weight (~10% by volume). After sonicating and shaking for 30 min, the solution was cast into Teflon cups, and the solvent was let to evaporate at room temperature. The films that formed inside Teflon cups were dried in vacuum oven at 100 °C for 3 days to remove all residual solvent. Samples were then molded into cylindrical geometry with 12 mm diameter and 5 mm height. The preadsorbed chains on nanoparticles are irreversibly adsorbed due to the high energy barrier. <sup>26,27</sup> This is important for the stability of interfacial layers and motivation of this study, as chemical heterogeneity within the interfacial layers are being investigated for their local viscosities.

**Thermal Analysis.** The amount of adsorbed polymer was determined via a TA Q50 thermogravimetric analyzer (TGA). Samples were preheated at 150 °C for 20 min. The heating rate was set to 5 °C/min, and the terminal temperature was set to 580 °C. A TA Q100 differential scanning calorimeter (DSC) was used to measure specific heat capacities. DSC experiments were performed at a heating rate of 10 °C/min between 0 and 120 °C. All samples were subjected to an initial heating/cooling cycle to erase their thermal histories. DSC data was collected after the first heating/cooling cycle after equilibrating all samples at 0 °C for 1 h. The specific heat capacities of all samples are presented in Figure S3.

Small-Angle X-ray Scattering (SAXS) Analysis. Small-angle X-ray scattering (SAXS) experiments were performed at the NSLS-II 12-ID beamline at Brookhaven National Laboratory. The sample to detector distance was 8.3 m, and data was collected at  $0.005-0.15~\text{\AA}^{-1}$  q range. NIKA software package<sup>28</sup> was employed to process two-dimensional (2D) SAXS data. One-dimensional (1D) SAXS plots were generated by integrating 2D SAXS data after background correction. The SAXS data was fitted by the Unified model,<sup>29</sup> as described in the Supporting Information.

Magnetic Heating Experiments. Magnetic heating experiments were carried out using an RDO HFI 3-135/400-3W magnetic heater

equipped with a heating coil having 3.75 turns, an inner diameter of 35 mm, and a pitch of 11 mm. The sample was placed at the center of the magnetic coil, and the region containing the sample and the magnetic coil was isolated from the environment with a thermal barrier to minimize heat loss. Samples were exposed to three different magnetic fields (see Table 2) during which the temperature ranged between 30 and 55 °C. Heating and cooling data was collected by a fiber optic sensor (Figure S6).

Table 2. Magnetic Heating Setup Conditions Used in Experiments

current (A)	voltage (V)	frequency, $f$ (kHz)	amplitude, $H_0$ (Oe)
33	16	240	37.5
76	24	230	86.5
142	35	225	161.5

## ■ RESULTS AND DISCUSSION

Density and Rigidity of Adsorbed Layers. Stress dissipation and rheological properties are governed by chain conformations and entanglements of interfacial layers. The entanglement density and chain packing within interfacial layers are strongly dependent on the rigidity of polymers. In this study, the local viscosity of the interfacial layers of chains with varying rigidity in poly(methyl acrylate) nanocomposites was investigated. We define chain rigidity, which is the local stiffness of a polymer chain, through Flory's characteristic ratio  $(C_{\infty})$ . The characteristic ratios of the adsorbed polymers used in the current study are between 8 and 10 (see Table 1). PVAc, PC, and P2VP have similar molecular weights (around 45 kDa). The two PMMA samples have molecular weights of 10 and 188 kDa, which are below and above the entanglement molecular weight of PMMA, respectively. The density of adsorbed PMMA chains was measured to be 16 chains/NP for 10 kDa and 3 chains/NP for 188 kDa. PMMA with 10 kDa has the highest chain density because the adsorption of short chains is energetically more favorable for this low molecular weight. All polymer-adsorbed particles were dispersed in 40 kDa PMA. The low glass transition temperature of PMA ( $T_{\rm g}$ : 15 °C) enables rotation and diffusion of particles during magnetic heating. The dispersion of nanoparticles in PMA at room temperature was characterized with small-angle X-ray scattering (SAXS) at NSLS-II, and 1D SAXS data was analyzed by the two-level unified function, which is a good model to analyze multiple-level structures.<sup>29</sup> The size obtained from fitting refers to  $R_{g}$ , which relates to size of a spherical particle by  $R_g = \sqrt{\frac{3}{5}}R$ . Thus, R from SAXS calculated as 7.7 nm is equivalent to particle size (7.5 nm) observed in transmission electron microscopy (TEM). The data at the low-q region, lower than 0.05  ${\hat A}^{'1}$ , indicates small clusters of 40 nm size. SAXS data of all samples are presented in Figure 1, along with the unified model fits. Radius of gyration  $(R_{o})$  and fractal dimension (p) values from the two-level unified fitting are listed in Table S1. P is determined from the slope of the SAXS profiles at the low-q regime and depends on the surface scattering and the shape of the aggregations. The second-level fractal dimension  $(p_2)$  varies in different samples. For the bare and PVAc composites,  $p_2 < 3$  indicates mass fractals; for PMMA and P2VP samples,  $p_2$ > 4 indicates diffusive interfaces; and for composite with PC, adsorbed layer has surface fractal,

where  $3 < p_2 < 4$ . The first-level fractal dimension  $(p_1)$  for

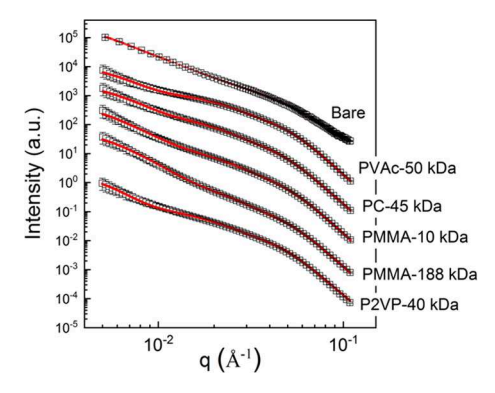


**Figure 1.** Small-angle X-ray scattering data of poly(methyl acrylate) (PMA) nanocomposites with 30 wt % Fe<sub>3</sub>O<sub>4</sub> nanoparticle loading shows that particle dispersion in PMA matrix polymer is not affected by the type and length of adsorbed polymers on particles. The two-level unified model fittings are shown with the red lines.

individual particle size analysis,  $p_1$ > 4 in all samples, is indicating the diffuse interface behavior at the particle level.

The interfacial dynamics can be observed with a specific heat capacity increase around the  $T_{\rm g}$  of the matrix polymer. The glassy layer thickness (h) was calculated from the measured heat capacities of composites ( $\Delta C_{\rm p,c}$ ) and bulk homopolymer ( $\Delta C_{\rm p,m}$ ) as follows

$$h = \left[ R^{3} + \frac{R^{3} \left( 1 - p - \frac{C_{p,c}}{C_{p,m}} \right) \rho_{NP}}{p \rho_{m}} \right]^{1/3} - R$$

where R is the NP radius, p is the NP weight fraction in nanocomposite,  $\rho_{\rm NP}$  is the NP density (5.2 g/cm³), and  $\rho_{\rm m}$  is the density of matrix polymer (PMA) (1.2 g/cm³). The above equation is derived and discussed in detail in the Supporting Information.

 $\Delta C_{\rm p}$  of composites with chemical heterogeneity in their interfacial layers have been corrected by subtracting the  $\Delta C_{\rm p}$  of pure Fe<sub>3</sub>O<sub>4</sub> nanoparticles. The glassy layer thickness (h), which varies between 1 and 3 nm, is consistent with glassy layer thicknesses reported in the literature. The glassy layer diminishes when rigidity (characteristic ratio,  $C_{\infty}$ ) of the adsorbed layer increases from 8 (for PMMA) to 10 (for P2VP), as shown in Table 3.

The shorter adsorbed chains can form a denser interfacial layer, and subsequently, can slow down the dynamics of matrix chains within the interphase region more effectively. PMMA with 10 kDa molecular weight showed the highest glassy layer thickness (3 nm). For less flexible adsorbed chains (P2VP and PC), glassy layer thicknesses were extremely low, which is

Table 3. Glassy Layer Thickness (h) and the Average Specific Heat Capacity ( $C_{\rm p,c}$ ) of Composites Measured Between 25 and 65 °C

sample	molecular weight (kDa)	$C_{\rm p,c}~({\rm J/g/^{\circ}C})$	h (nm)
PMMA	10	1.4	$3.0 \pm 1.3$
PMMA	188	1.4	$2.5 \pm 1.1$
PVAc	50	1.4	$1.1 \pm 0.6$
PC	45	1.4	0
P2VP	40	1.6	0
Bare	40	1.5	$1.5 \pm 0.47$

believed to be due to the weak interactions between these chains and the matrix polymer PMA. Density and packing of chains close to nanoparticles were found to increase with decreasing chain length. The lower elastic modulus of P2VP-adsorbed particles reported in our previous work also indicated the existence of the tightly bounded adsorbed layer, where interactions between adsorbed and matrix chains are considered to be weak. Polymer rigidity was shown to be an important molecular parameter for the conformational interactions, interfacial mixing, and dynamics between two miscible polymers with dynamic asymmetries.

Adsorbed chains and their conformations influence the hydrodynamic sizes of nanoparticles. By measuring the nanoparticle diffusion in polymer melts, an effective hydrodynamic size of particles can be obtained. It was found that strongly adsorbed P2VP chains on SiO<sub>2</sub> nanoparticles can exhibit extended chains up to their  $R_g$  within an effective hydrodynamic size. <sup>22,31</sup> Because PMA composite with bare Fe<sub>3</sub>O<sub>4</sub> nanoparticles is attractive as in the case of P2VP-SiO<sub>2</sub> composite, the hydrodynamic layer thickness (L) is assumed to be at the length scale of the  $R_g$  of PMA (8 nm). For all our composites except those containing PMMA, the hydrodynamic size of particles in 40 kDa PMA was calculated by adding the  $R_{\rm g}$  of PMA (8 nm) to the particle radius (7.5 nm). In the case of PMMA-adsorbed particles, an additional 3 nm is added to the hydrodynamic radius to account for the glassy layer thickness. Topological constraints from the entanglements between mixing of PMMA and PMA may influence the hydrodynamic size of particles, but we assume that the hydrodynamic size in all PMA composites remains the same. We discuss the foreseen interfacial effects on the measured viscosities of different samples in the following section.

Magnetic Heating. Magnetic nanoparticles and their magnetic moments rotate to align with applied magnetic fields due to Brownian and Néelian relaxations, respectively. 32-35 In magnetic susceptibility measurements, the rotational Brownian relaxation time is the reciprocal of the frequency associated with the peak of the imaginary susceptibility,  $\chi''$  33,34 In magnetic heating experiment, the energy dissipation due to both Brownian and Néel relaxation processes is monitored by temperature change as a function of time. A polynomial fitting is applied to the heating and cooling rate data.  $\left(\frac{dT_h}{dt}\right)$  and  $\left(\frac{dT_c}{dt}\right)$ are the first derivatives of the fitted function. The heating rate data with their polynomial fittings are shown in Figure S4. We subtracted the cooling rate (due to heat loss to the environment),  $\frac{dT_c}{dt}$ , from the heating rate,  $\frac{dT_h}{dt}$ , to determine the absolute heating rate,  $\left(\frac{dT}{dt}\right)_a$ . Figure 2 is the representative integrated data between 33.5 and 43.0 °C for three different alternating magnetic fields. As seen, the heat loss is negligible at 86.45 and 161.53 Oe since the heating rates are quite high at these high magnetic amplitudes. Magnetic heating rates and magnetic heating raw data of the other samples are given in Figures S5 and S6.

Specific energy absorption rate (SAR) is the rate of electromagnetic energy absorbed by the viscous polymer solution and is expressed by the equation SAR =  $\left(\frac{dT}{dt}\right)_a \frac{C_{p,c}}{p}$ , where  $C_{p,c}$  is the specific heat capacity of polymer nanocomposite and p is the nanoparticle weight fraction. The magnetic heating data was analyzed using the power

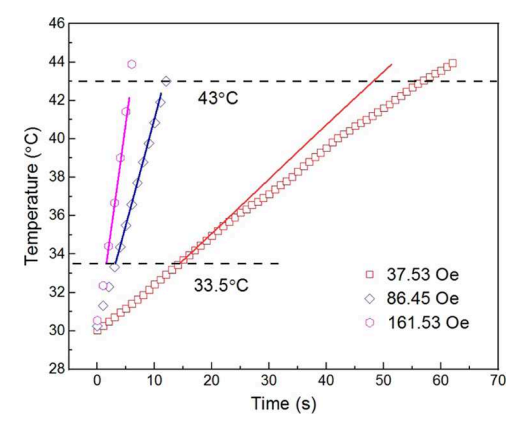


**Figure 2.** Magnetic heating rate of PMA nanocomposites with bare Fe<sub>3</sub>O<sub>4</sub> particles at 30 wt % loading at three different field amplitudes. The solid lines represent the absolute heating rate after subtracting the cooling rate.

dissipation model to obtain the effective relaxation times  $(\tau)$ .  $^{35,37}$ 

$$\begin{aligned} \mathrm{SAR}(d) &= \int_{\infty}^{0} \mu_0 f \pi H_0^2 \chi_0 \frac{2\pi f \tau}{\left(2\pi f \tau\right)^2 + 1} \times \frac{1}{w \sqrt{(\pi/2)}} \\ &= \exp \left(-2 \left(\frac{d - d_0}{w}\right)^2\right) \mathrm{d}d \end{aligned}$$

where  $\mu_0$  is the vacuum permeability, f is the frequency of the applied magnetic field,  $H_0$  is the field amplitude,  $\chi_0$  is the equilibrium susceptibility, w is the size-distribution width, and  $d_0$  is the average particle diameter.  $\tau$  is the sum of rotational Brownian relaxation time  $(\tau_{\rm B})$  and Néel relaxation time  $(\tau_{\rm N})$  as follows

$$\frac{1}{\tau} = \frac{1}{\tau_{\rm B}} + \frac{1}{\tau_{\rm N}}$$

Figure 3A shows SAR as a function of temperature at three different magnetic fields in bare  $\text{Fe}_3\text{O}_4/\text{PMA}$  composite. The linear relationship between average SAR and field amplitude squared,  $H_0^2$ , is shown in Figure 3A inset. Averaged bare particle diameter is 15 nm with a size dispersity (w) of 3 nm as determined via transmission electron microscopy (Figure S7). Under weak magnetic fields at room temperature, the effect of Néelian relaxations is negligible. Therefore, the effective relaxation time for the Brownian relaxations can be calculated from the Stokes–Einstein relationship

$$\tau = \tau_{\rm B} = \frac{3\eta V_{\rm h}}{k_{\rm B}T}$$

where  $k_{\rm B}$  is the Boltzmann constant, T is the temperature,  $\eta$  is the viscosity of the medium, and  $V_{\rm h}$  is the hydrodynamic volume of particles, calculated by  $V_{\rm h}=\frac{4}{3}\pi(R+L)^3$ , where L is the hydrodynamic layer thickness and R is the NP radius. The viscosity of the interphase around Fe<sub>3</sub>O<sub>4</sub> NPs as a function of angular frequency ( $\omega=1/\tau_{\rm B}$ ) and temperature (T) is illustrated in Figure 3B. The physical parameters used in the viscosity calculations are listed in Tables S1 and S2. At 35 °C, the rotational Brownian relaxation times of Fe<sub>3</sub>O<sub>4</sub> NPs in different samples are plotted as a function of adsorbed chain rigidity (Figure 3C). Among the composites with heterogeneous interphases, the longest relaxation time is obtained with

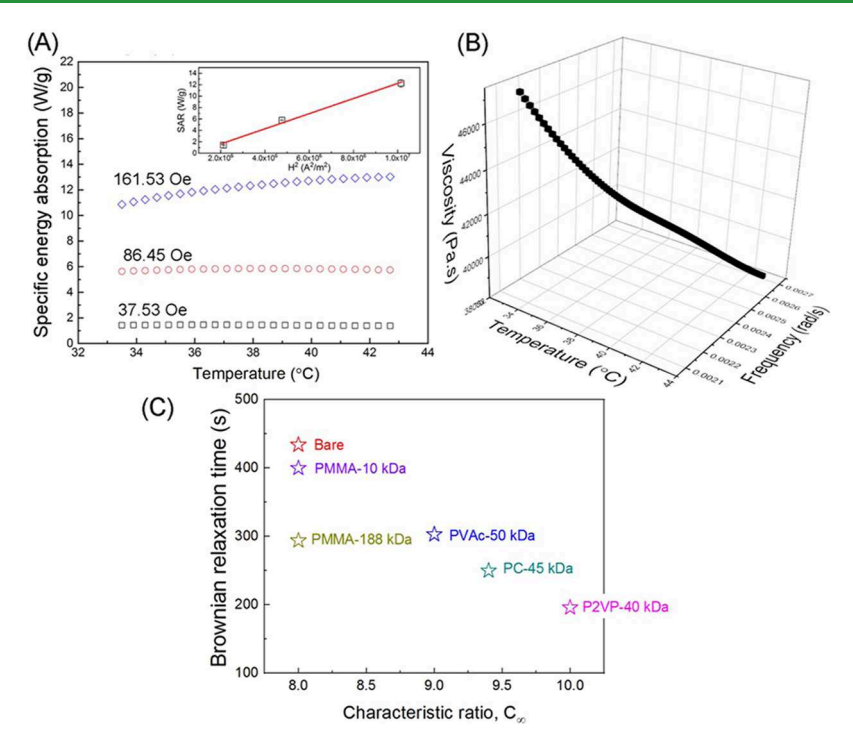


Figure 3. (A) Specific energy absorption rate (SAR) as a function of temperature for PMA composites with bare  $Fe_3O_4$  NPs at 30% loading at three different magnetic field amplitudes ( $H_0$ ). The inset shows the linear dependency of averaged SAR on  $H_0^2$ . (B) Calculated viscosity of bare PMA composite as a function of temperature and angular frequency. (C) Rotational Brownian relaxation time of  $Fe_3O_4$  NPs adsorbed with polymers of different rigidities at 35 °C.

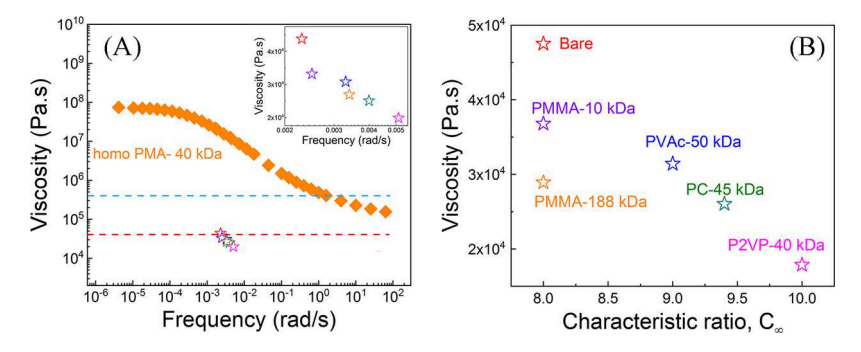


Figure 4. (A) Calculated viscosity measured at different frequencies for all PMA nanocomposites with different adsorbed polymer types and rigidities in chemically heterogeneous interfaces. Viscosity data of PMA homopolymer (40 kDa) is shown in orange. The reference temperature is 35 °C. (B) Calculated viscosities of all composites from magnetic heating experiments for varying rigidities of polymers in interfacial layers at 35 °C.

10 kDa PMMA, and the relaxation time decreases with adsorbed chain rigidity. Figure S8 shows the calculated viscosities of all samples at different temperatures. Note that bare composite viscosity decays with temperature, but the viscosity of polymer-adsorbed particle composites do not decrease at the same rate, rather increase or remain steady around 40–42 °C. Data presented in Figure 3 is for 35 °C.

The rotational diffusivity of particles occurs in low-molecular-weight polymers. In previous work, the rotational diffusivity of ferrite nanoparticles in polymer melts was measured faster than the Stokes–Einstein prediction in high-molecular-weight polymer whose contour length is larger than particle hydrodynamic size.<sup>34</sup> In this study, we showed that the rotation of particles is not restricted by molecular weights and entanglements. Calculated viscosities of composites were found to be lower than the viscosity of bulk PMA homopolymer, measured in a rheometer (Figure 4A). The

critical molecular weight  $(M_c)$  of PMA is 18 kDa  $(M_c \approx$  $2M_e$ ).<sup>38</sup> For molecular weights above  $M_c$ , the zero-shear viscosity is estimated by  $\eta_0 = \log_{10}(C_2)M^{3.4}$ . Using  $\eta_0$  for 40 kDa PMA homopolymer (2.75  $\times$  10<sup>7</sup> Pa·s),  $C_2$  is calculated to be -8.21. For unentangled state,  $M < M_{\odot}$  the zero-shear viscosity is calculated by  $\eta_0 = \log_{10}(C_1)M$ . At  $M = M_o$ ,  $\eta_0$  of the two regimes are equal, which gives  $C_1 = 2$ . After substituting  $C_1$ and  $C_2$  constants into  $\eta_0$  equations for the unentangled and entangled cases,  $\eta_0$  of unentangled PMA is calculated as 4.0  $\times$ 10<sup>6</sup> Pa·s (blue line on Figure 4A). It has been proposed that the hydrodynamic resistance to translation and rotation is determined by the local viscosity influenced by segmental friction.<sup>39</sup> The deviations from the rotational diffusivity of a particle in a polymer melt arise from these chain segments. The nonlocal constitutive equation for the segment viscosity  $(\eta_s)$  in unentangled polymer melts is described as

where  $\eta_{\rm b}$  is the macroscopic bulk polymer viscosity and q is the wave vector for the velocity gradients around particles. Assuming that  $q \sim 2/D_{\rm h}$  and  $\eta_s = \eta_{\rm e}$ , the above equation can also be written as  $\frac{\eta_{\rm b}}{\eta_{\rm c}} = 1 + \left(\frac{2R_{\rm g}}{D_{\rm h}}\right)^2$ . According to Ganesan et al.,<sup>39</sup> when the ratio of radius of gyration to particle hydrodynamic radius exceeds unity, the deviation to Stokes diffusion is observed. In another work by Berg et al.,<sup>40</sup> it is proposed that the ratio of melt polymer contour length to particle hydrodynamic size should exceed unity. A decrease of local viscosity around a spinning particle is observed when  $L_{\rm c}/D_{\rm h} \sim 1$ . Then, the ratio of viscosity is described as  $\frac{\eta_0}{\eta_{\rm local}} = 1 + \left(\frac{L_{\rm c}}{D_{\rm h}}\right)^2$ .  $\eta_0$  is the zero-shear viscosity of the bulk polymer matrix,  $\eta_{\rm local}$  is the viscosity of the interphase around NPs,  $L_{\rm c}$  is the contour length of PMA chains, and  $d_{\rm h}$  is the hydrodynamic diameter of NPs.

In our PMA composites, the hydrodynamic diameter of particles is 31 nm. The  $L_{\rm c}$  of 40 kDa PMA is calculated to be 263.64 nm (= Nb), where N is the number of Kuhn segments and b is the Kuhn length (1.5 nm). By substituting the measured  $\eta_0$  for unentangled state,  $\eta_{local}$  is calculated to be 4.0  $\times$  10<sup>4</sup> Pa·s, which matches the viscosity for the bare composite from the magnetic heating experiment. Thus, this analysis supports that our local viscosity analysis based on the magnetic heating data is reliable. The frequency of the rotational Brownian motion measured from our samples is around 0.0023 rad/s, which is close to the frequency (0.0024 rad/s) of 16 nm diameter grafted ferrite particles in PEG melts at 308 K.34 A good agreement between our magnetic heating results and dynamic susceptibility measurements verifies that the classic energy dissipation model commonly used in ferrofluids can be used to study polymer fluids.

Figure 4B shows the viscosities for our samples with different rigidities in adsorbed layers. The lowest interfacial viscosities are for the PC and P2VP-adsorbed particles. Particles rotate easily in weak interfaces with negligible restricted mobility when it is compared to the other composites with strong interfaces, where the adsorbed and matrix chains mix and entangle. The viscosity of the composites increases with the decreasing rigidity of adsorbed polymers. These findings are consistent with the rheology results of PEO and PMA composite systems, where more flexible adsorbed chains were reported to have better reinforcement. In addition, the nonlinear experiments showed that at 180 °C nanocomposite with the PMMA-adsorbed chains exhibited higher viscoelastic properties after deformation, whereas composites with P2VP-adsorbed chains slightly softened after large-amplitude oscillatory strain (LAOS) application. Because of the deformability of the adsorbed PMMA layer, the interface layer was called "diffuse" interface. Hence, the matrix (PEO) chains can diffuse into the loosely bound PMMA layer. Viscosities measured from the magnetic heating experiments are attributed to the strong and weak interfacial layers, where chain conformations are different, and this difference in mixing and viscosity is explained by the rigidity of chains on nanoparticles. The postulated adsorbed chain conformations of PMMA and P2VP samples<sup>4</sup> are supported with the local viscosities measured in this work.

### CONCLUSIONS

Chemical heterogeneities within interfacial layers around nanoparticles are used to explore the rheological behavior of nanocomposites, going beyond the general understanding of slow dynamics of immobilized glassy layers. While asymmetry in dynamics of polymer blends is intriguing and can be utilized in unique material designs with different polymer architectures, their dynamics will be different when they are on nanoparticles. Thus, the dynamics of the interfacial layers becomes critically important for polymer nanocomposite applications. Chain conformations in interfacial layers were previously proposed to control the linear rheological properties and their nonlinear responses, which were designed to explain the deformability and recovery of interfacial mixing and re-entanglements in our composites. This study is designed to measure the local viscosity around nanoparticles in a low- $T_g$  matrix polymer (PMA matrix loaded with Fe<sub>3</sub>O<sub>4</sub> nanoparticles). The rotational motion of nanoparticles in the polymer melt was found to be less affected by the polymer entanglement network than their translational motion. As a result, the magnetic nanoparticles in polymer melt experienced viscosities that are lower than the zero-shear rate viscosity of unentangled PMA melt ( $\eta_0 = 4.0 \times$ 106 Pa·s). Spinning and rotating particles did not feel the resistance of the entangled matrix chains when adsorbed chains were rigid (such as PC and P2VP). The local viscosity increased systematically with decreasing adsorbed chain rigidity. The highest local viscosity was measured with the short adsorbed (PMMA) chains because of the dense interfacial layer between PMA and PMMA. Polymer nanocomposites with magnetic fillers presented in this work use the magnetic heating concept to measure the viscosity of composites. The internal heating of magnetic nanocomposites and their interfacial layer-controlled viscosities could be utilized for drug delivery systems but more importantly for flexible electromagnetic actuator membrane designs.

# ASSOCIATED CONTENT

# Supporting Information

The Supporting Information is available free of charge at https://pubs.acs.org/doi/10.1021/acsapm.0c00889.

Unified model fitting parameters; FTIR spectra of  $Fe_3O_4$  nanoparticles; TGA data of polymer-adsorbed nanoparticles; heat capacities of PMA homopolymer and its nanocomposites; magnetic heating/cooling data; particle size distribution; viscosities as a function of temperature; magnetic characteristics of PMA nanocomposites; parameters used in magnetic heating data analysis; and viscosities of PMA nanocomposites measured in a rheometer (PDF)

## AUTHOR INFORMATION

#### **Corresponding Author**

Pinar Akcora — Department of Chemical Engineering & Materials Science, Stevens Institute of Technology, Hoboken, New Jersey 07030, United States; ○ orcid.org/0000-0001-7853-7201; Email: pakcora@stevens.edu

## Authors

Di Wu − Department of Chemical Engineering & Materials Science, Stevens Institute of Technology, Hoboken, New Jersey 07030, United States

- Donovan G. Weiblen Department of Materials Science and Engineering, Rensselaer Polytechnic Institute, Troy, New York 12180, United States
- Rahmi Ozisik Department of Materials Science and Engineering, Rensselaer Polytechnic Institute, Troy, New York 12180, United States; orcid.org/0000-0002-8936-5158

Complete contact information is available at: https://pubs.acs.org/10.1021/acsapm.0c00889

## **Author Contributions**

The manuscript was written through the contributions of all authors.

## **Funding**

This material is based upon the work supported by the National Science Foundation CMMI MEP program under Grant nos. 1825250 and 1825254.

#### Notes

The authors declare no competing financial interest.

#### REFERENCES

- (1) Cao, L.; Wang, Y.; Dong, P.; Vinod, S.; Tijerina, J. T.; Ajayan, P. M.; Xu, Z.; Lou, J. Interphase Induced Dynamic Self-Stiffening in Graphene-Based Polydimethylsiloxane Nanocomposites. *Small* **2016**, *12*, 3723–3731.
- (2) Cudjoe, E.; Khani, S.; Way, A. E.; Hore, M. J. A.; Maia, J.; Rowan, S. J. Biomimetic Reversible Heat-Stiffening Polymer Nanocomposites. *ACS Cent. Sci.* **2017**, *3*, 886–894.
- (3) Wood, C. D.; Chen, L.; Burkhart, C.; Putz, K. W.; Torkelson, J. M.; Brinson, L. C. Measuring interphase stiffening effects in styrene-based polymeric thin films. *Polymer* **2015**, *75*, 161–167.
- (4) Yang, S.; Hassan, M.; Akcora, P. Role of adsorbed chain rigidity in reinforcement of polymer nanocomposites. *J. Polym. Sci., Part B: Polym. Phys.* **2019**, *57*, 9–14.
- (Ś) Yang, S.; Akcora, P. Deformation of Chemically Heterogeneous Interfacial Layers of Polymer Nanocomposites. *ACS Macro Lett.* **2019**, *8*, 1635–1641.
- (6) Senses, E.; Akcora, P. Tuning mechanical properties of nanocomposites with bimodal polymer bound layers. *RSC Adv.* **2014**, *4*, 49628–49634.
- (7) Yang, S.; Liu, S.; Narayanan, S.; Zhang, C.; Akcora, P. Chemical heterogeneity in interfacial layers of polymer nanocomposites. *Soft Matter* **2018**, *14*, 4784–4791.
- (8) Brodeck, M.; Alvarez, F.; Moreno, A. J.; Colmenero, J.; Richter, D. Chain motion in nonentangled dynamically asymmetric polymer blends: Comparison between atomistic simulations of PEO/PMMA and a generic bead-spring model. *Macromolecules* **2010**, *43*, 3036–3051.
- (9) Haley, J. C.; Lodge, T. P. Dynamics of a poly(ethylene oxide) tracer in a poly(methyl methacrylate) matrix: Remarkable decoupling of local and global motions. *J. Chem. Phys.* **2005**, *122*, No. 234914.
- (10) Ito, H.; Russell, T. P.; Wignall, G. D. Interactions in Mixtures of Poly(ethylene oxide) and Poly(methyl methacrylate). *Macromolecules* 1987, 20, 2213–2220.
- (11) Lutz, T. R.; He, Y.; Ediger, M. D.; Cao, H.; Lin, G.; Jones, A. A. Rapid poly(ethylene oxide) segmental dynamics in blends with poly(methyl methacrylate). *Macromolecules* **2003**, *36*, 1724–1730.
- (12) Niedzwiedz, K.; Wischnewski, A.; Monkenbusch, M.; Richter, D.; Genix, A. C.; Arbe, A.; Colmenero, J.; Strauch, M.; Straube, E. Polymer chain dynamics in a random environment: Heterogeneous mobilities. *Phys. Rev. Lett.* **2007**, *98*, No. 168301.
- (13) Pedemonte, E.; Polleri, V.; Turturro, A.; Cimmino, S.; Silvestre, C.; Martuscelli, E. Thermodynamics of poly(ethylene oxide)-poly(methyl methacrylate) blends: prediction of miscibility based on the corresponding-states theory. *Polymer* **1994**, 35, 3278–3281.

- (14) Senses, E.; Isherwood, A.; Akcora, P. Reversible Thermal Stiffening in Polymer Nanocomposites. *ACS Appl. Mater. Interfaces* **2015**, *7*, 14682–14689.
- (15) Senses, E.; Faraone, A.; Akcora, P. Microscopic Chain Motion in Polymer Nanocomposites with Dynamically Asymmetric Interphases. *Sci. Rep.* **2016**, *6*, No. 29326.
- (16) Cheng, S.; Holt, A. P.; Wang, H.; Fan, F.; Bocharova, V.; Martin, H.; Etampawala, T.; White, B. T.; Saito, T.; Kang, N.-G.; Dadmun, M. D.; Mays, J. W.; Sokolov, A. P. Unexpected Molecular Weight Effect in Polymer Nanocomposites. *Phys. Rev. Lett.* **2016**, *116*, No. 038302.
- (17) Cheng, S.; Bocharova, V.; Belianinov, A.; Xiong, S.; Kisliuk, A.; Somnath, S.; Holt, A. P.; Ovchinnikova, O. S.; Jesse, S.; Martin, H.; Etampawala, T.; Dadmun, M.; Sokolov, A. P. Unraveling the Mechanism of Nanoscale Mechanical Reinforcement in Glassy Polymer Nanocomposites. *Nano Lett.* **2016**, *16*, 3630–3637.
- (18) Cheng, S.; Carroll, B.; Lu, W.; Fan, F.; Carrillo, J. M. Y.; Martin, H.; Holt, A. P.; Kang, N. G.; Bocharova, V.; Mays, J. W.; Sumpter, B. G.; Dadmun, M.; Sokolov, A. P. Interfacial Properties of Polymer Nanocomposites: Role of Chain Rigidity and Dynamic Heterogeneity Length Scale. *Macromolecules* **2017**, *50*, 2397–2406.
- (19) Friedenberg, M. C.; Mate, C. M. Dynamic Viscoelastic Properties of Liquid Polymer Films Studied by Atomic Force Microscopy. *Langmuir* **1996**, *12*, 6138–6142.
- (20) Gelbert, M.; Roters, A.; Schimmel, M.; Rühe, J.; Johannsmann, D. Viscoelastic spectra of soft polymer interfaces obtained by noise analysis of AFM cantilevers. *Surf. Interface Anal.* **1999**, *27*, 572–577.
- (21) Grabowski, C. A.; Mukhopadhyay, A. Size Effect of Nanoparticle Diffusion in a Polymer Melt. *Macromolecules* **2014**, 47, 7238–7242.
- (22) Bailey, E. J.; Griffin, P. J.; Composto, R. J.; Winey, K. I. Characterizing the Areal Density and Desorption Kinetics of Physically Adsorbed Polymer in Polymer Nanocomposite Melts. *Macromolecules* **2020**, *53*, 2744–2753.
- (23) Brochard Wyart, F.; de Gennes, P. G. Viscosity at small scales in polymer melts. *Eur. Phys. J. E: Soft Matter Biol. Phys.* **2000**, *1*, 93–97.
- (24) Cai, L.-H.; Panyukov, S.; Rubinstein, M. Mobility of Nonsticky Nanoparticles in Polymer Liquids. *Macromolecules* **2011**, 44, 7853–7863.
- (25) You, W.; Yu, W. Slow Linear Viscoelastic Relaxation of Polymer Nanocomposites: Contribution from Confined Diffusion of Nanoparticles. *Macromolecules* **2019**, *52*, 9094–9104.
- (26) Monnier, X.; Napolitano, S.; Cangialosi, D. Direct observation of desorption of a melt of long polymer chains. *Nat. Commun.* **2020**, *11*, No. 4354.
- (27) Napolitano, S. Irreversible adsorption of polymer melts and nanoconfinement effects. *Soft Matter* **2020**, *16*, 5348–5365.
- (28) Ilavsky, J. Nika: software for two-dimensional data reduction. *J. Appl. Crystallogr.* **2012**, *45*, 324–328.
- (29) Beaucage, G. Approximations Leading to a Unified Exponential/Power-Law Approach to Small-Angle Scattering. *J. Appl. Crystallogr.* **1995**, 28, 717–728.
- (30) Sargsyan, A.; Tonoyan, A.; Davtyan, S.; Schick, C. The amount of immobilized polymer in PMMA SiO2 nanocomposites determined from calorimetric data. *Eur. Polym. J.* **2007**, *43*, 3113–3127.
- (31) Griffin, P. J.; Bocharova, V.; Middleton, L. R.; Composto, R. J.; Clarke, N.; Schweizer, K. S.; Winey, K. I. Influence of the Bound Polymer Layer on Nanoparticle Diffusion in Polymer Melts. *ACS Macro Lett.* **2016**, *5*, 1141–1145.
- (32) Dieckhoff, J.; Eberbeck, D.; Schilling, M.; Ludwig, F. Magnetic-field dependence of Brownian and Néel relaxation times. *J. Appl. Phys.* **2016**, *119*, No. 043903.
- (33) Fannin, P. C.; Charles, S. W. The study of a ferrofluid exhibiting both Brownian and Neel relaxation. *J. Phys. D: Appl. Phys.* **1989**, 22, 187–191.
- (34) Maldonado-Camargo, L.; Rinaldi, C. Breakdown of the Stokes-Einstein Relation for the Rotational Diffusivity of Polymer

- Grafted Nanoparticles in Polymer Melts. *Nano Lett.* **2016**, *16*, 6767–6773.
- (35) Torres, T. E.; Lima, E.; Calatayud, M. P.; Sanz, B.; Ibarra, A.; Fernández-Pacheco, R.; Mayoral, A.; Marquina, C.; Ibarra, M. R.; Goya, G. F. The relevance of Brownian relaxation as power absorption mechanism in Magnetic Hyperthermia. *Sci. Rep.* **2019**, *9*, No. 3992.
- (36) Nemala, H.; Thakur, J. S.; Naik, V. M.; Vaishnava, P. P.; Lawes, G.; Naik, R. Investigation of magnetic properties of Fe3O4 nanoparticles using temperature dependent magnetic hyperthermia in ferrofluids. *J. Appl. Phys.* **2014**, *116*, No. 034309.
- (37) Rosensweig, R. E. Heating magnetic fluid with alternating magnetic field. J. Magn. Magn. Mater. 2002, 252, 370-374.
- (38) Wu, S. Predicting chain conformation and entanglement of polymers from chemical structure. *Polym. Eng. Sci.* **1992**, 32, 823–830.
- (39) Ganesan, V.; Pryamitsyn, V.; Surve, M.; Narayanan, B. Noncontinuum effects in nanoparticle dynamics in polymers. *J. Chem. Phys.* **2006**, *124*, No. 221102.
- (40) Sluch, M. I.; Somoza, M. M.; Berg, M. A. Friction on small objects and the breakdown of hydrodynamics in solution: Rotation of anthracene in poly(isobutylene) from the small-molecule to polymer limits. *J. Phys. Chem. B* **2002**, *106*, 7385–7397.